JOURNAL OF GEOPHYSICAL RESEARCH, VOL. 114, B11203, doi:10.1029/2008JB006216, 2009

Transport capacity of pyroclastic density currents: Experiments and models of substrate-flow interaction

Josef Dufek,[1] Jason Wexler,[2] and Michael Manga[2]

Received 18 November 2008; revised 20 June 2009; accepted 23 July 2009; published 7 November 2009.

[1] One of the more distinctive features of many ignimbrites is the presence of large lithics (some greater than meter scale) and pumices that have been transported great distances (>10 km) from the eruptive vent, sometimes over steep terrain and expanses of water. In many cases, these particles have been transported much further than can be explained by aerodynamic forces and ballistic trajectories. We examine the forces responsible for transport of large clasts and examine in detail the momentum transfer occurring when particles interact with their boundaries. We performed a suite of experiments and numerical simulations to quantify the mass and momentum transfer that occurs when particles interact with a pumice bed substrate and with water substrate, two geologically motivated flow end-members. We find that clasts transported in dilute currents are particularly sensitive to the nature of the boundary, and while large particles can skip several times on a water substrate, they travel less far than particles that impact pumice bed substrates. All else being equal, large particles in dense pyroclastic density currents are themselves relatively insensitive to the details of their boundaries; however, one of the most important ways boundary conditions influence large particles is not through direct interaction but by changing the local concentration of fine particles. Momentum transfer from fine particles to large particles appears to be required to transport large clasts great distances. If initially dense flows become dilute during transport, then the transport capacity of large particles in the flow is substantially decreased.

Citation: Dufek, J., J. Wexler, and M. Manga (2009), Transport capacity of pyroclastic density currents: Experiments and models of substrate-flow interaction, *J. Geophys. Res.*, *114*, B11203, doi:10.1029/2008JB006216.

1. Introduction

[2] Pyroclastic density currents produced during explosive volcanic eruptions have some of the broadest grain size distributions of any geophysical, particle-laden gravity currents. For example, the maximum clast sizes and the distance these clasts are transported in such ground-hugging flows often far exceed those from turbidity currents, dust storms, and avalanches [*Branney and Kokelaar*, 2002; *Kneller et al.*, 1999; *Simpson*, 1997]. While large pumice and lithic clasts (>1 cm) are common in most ignimbrites (e.g., Figure 1), the specific transport mechanisms remain ambiguous. Yet, the granular and fluid forces responsible for the transport of large clasts are also responsible for macroscale flow properties such as runout distance. Ash-sized particles (diameters less than 2 mm) likely dominate the mass and momentum budget of these flows [*Sparks et al.*, 1991; *Valentine and Wohletz*, 1989], but large clasts provide a record of the forces internal to the flows and their segregation and transport has long been used for qualitative and quantitative inferences about pyroclastic density current dynamics [*Allen*, 2001; *Cagnoli and Magna*, 2005; *Dufek and Bergantz*, 2007a; *Fisher et al.*, 1993; *Palladino and Valentine*, 1995]. These flows are inherently difficult to observe in real time due to the hazard they present and the small optical depths of the granular mixture. Moreover, the largest-scale pyroclastic density currents have not been witnessed in historic times. A specific accounting of the forces necessary for the transport of clasts provides one of the few clues to the dynamics of these high-energy granular flows.

[3] The relative abundance of large clasts in deposits depends on both the source conditions (e.g., conduit fragmentation, conduit erosion) and the transport capacity of the individual pyroclastic density currents. In general, three types of effects may be responsible for the transport capacity of particles in these flows: 1. Interaction of particles with the gas phase (drag); 2. Interaction of particles with other particles (collisional and frictional); 3. Interaction of particles with the bed. However, transmission of energy in these flows can follow complex pathways and will depend on interactions between the three sets of processes. For example, particle-gas drag on small particles will, in part, determine the concentration of small particles, which can then interact with the larger clasts.

[4] One approach to understanding these forcings is to compare flows in which one of these interactions is isolated

[1]School of Earth and Atmospheric Sciences, Georgia Institute of Technology, Atlanta, Georgia, USA.
[2]Department of Earth and Planetary Science, University of California, Berkeley, California, USA.

0148-0227/09/2008JB006216$09.00

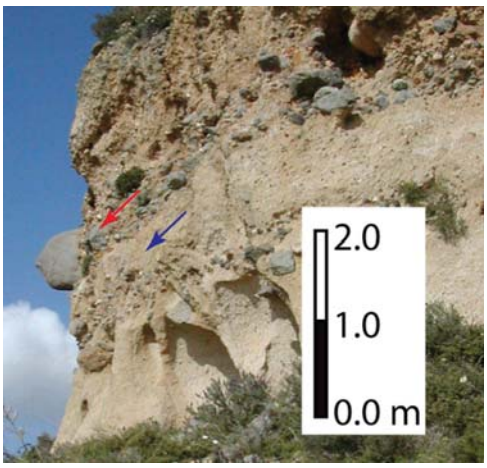

Figure 1. Lithics at the base of an ignimbrite unit on Kos, Greece. Many lithics exceed 50 cm at this location ~10 km from the source [*Allen et al.*, 1999]. The red arrow denotes a lithic enriched region, and the blue arrow denotes a pumice enriched region of this deposit. The pumice in this deposit is rhyolitic, and the majority of the accessory lithic clasts are andesitic and are likely derived from proximal vent erosion.

or emphasized. For instance, the transport of pyroclastic density currents over water and over land provides information about the role of the substrate boundary conditions in the transport of these flows. The proximity of many eruptions to the sea has resulted in numerous flows that have traversed bodies of water [*Allen and Cas*, 2001; *Burgisser*, 2005; *Carey et al.*, 1996; *Miller and Smith*, 1977] and many other flows have likely occurred but lack subaerial deposits. We have previously described the role of saltation in overland flows in developing a particle-concentrated bed load where particles make enduring and repeated contact with the bed, and compared these with over-water flows that fail to produce a bed load. However, we previously considered an end-member condition for over-water flows in which all particles that reach the basal boundary are removed from the flow. While this completely "leaky" boundary may describe well the interaction of ash-sized particles with water due to the role of surface tension, there are instances in which larger particles are not immediately removed; instead they skip along the surface. The precise energy and mass balance for this particle-water interaction was previously unknown, although previous experiments have been conducted on rock-skipping phenomena and military applications of bombs rebounding from a water surface [*Clanet et al.*, 2004; *Johnson*, 1998]. Likewise, a detailed accounting for the energy lost when particles encounter surfaces with roughnesses similar to the size of the impacting particle remain relatively poorly constrained. Indeed, particle-bed interaction is one of the major uncertainties in conceptual and numerical models of pyroclastic density current transport.

[5] Here we quantify the transport capacity of large clasts in the continuum of dense to dilute flows that comprise pyroclastic density currents, through an improved understanding of particle-particle interaction and flow feedback from more realistic boundary conditions.

[6] In section 2 we describe a series of particle-scale experiments aimed at improving our description of particle-bed interaction for both water and pumice bed substrates. Section 3 describes the results of these experiments, and in section 4 we construct a simplified model in which the effect of particle-concentration, particle-gas drag, and the boundary conditions can artificially be separated to better understand the role each of these interactions plays in isolation. We then examine the feedback between the substrate, particle concentration, and transport capacity of large clasts using a multiphase modeling approach in section 5 and apply this to an analysis of ignimbrite deposits in section 6.

2. Experimental Determination of Pumice Bed and Water Boundaries

[7] In a series of laboratory experiments, we measured the momentum exchange when particles encounter two types of substrate: water and a bed of pumice. We performed a series of 155 experiments in which we propelled pumice particles at a basin of water, and recorded the interaction with a high-speed video camera. Additionally, we performed an analogous series of 74 experiments to determine the interaction of pumice particles colliding with a bed of stationary pumice particles. The particles in the bed are identical in composition and size to the projectile particles used in both series of experiments; they are obtained from an air fall deposit of Medicine Lake Volcano, CA that has been sieved through a 9.5 to 12.5 mm sieve. The pumice particles vary significantly in mass, from 0.4 to 1.2 g, and come in a variety of shapes, from angular and oblong to nearly spherical. We choose these particles because we have previously made complementary measurements of the restitution coefficient [*Cagnoli and Manga*, 2003] and heat transfer to water [*Dufek et al.*, 2007] using particles from the same source. While other substrates are certainly possible, we focus here on collisions between materials that have similar surface roughnesses. These macroscale particles also enable a detailed accounting of the momentum balance.

[8] Figure 2 shows the experimental apparatus. We propel the particles from a gun powered by compressed nitrogen gas. By controlling the pressure of the gas, we can systematically vary the velocity of the pumice particle to understand how velocity affects the pumice-substrate interactions. We can achieve a range of velocities from 10 m/s up to

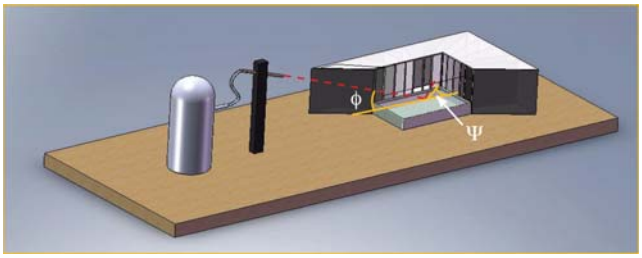

Figure 2. Experimental setup. Compressed nitrogen propels a pumice particle toward a reservoir of either water or pumice of similar diameter. A high-speed video camera records both the preimpact and postimpact velocities. To determine out-of-plane effects, a multicollector with different bins is used to determine the yaw angle when the particle leaves the bed surface.

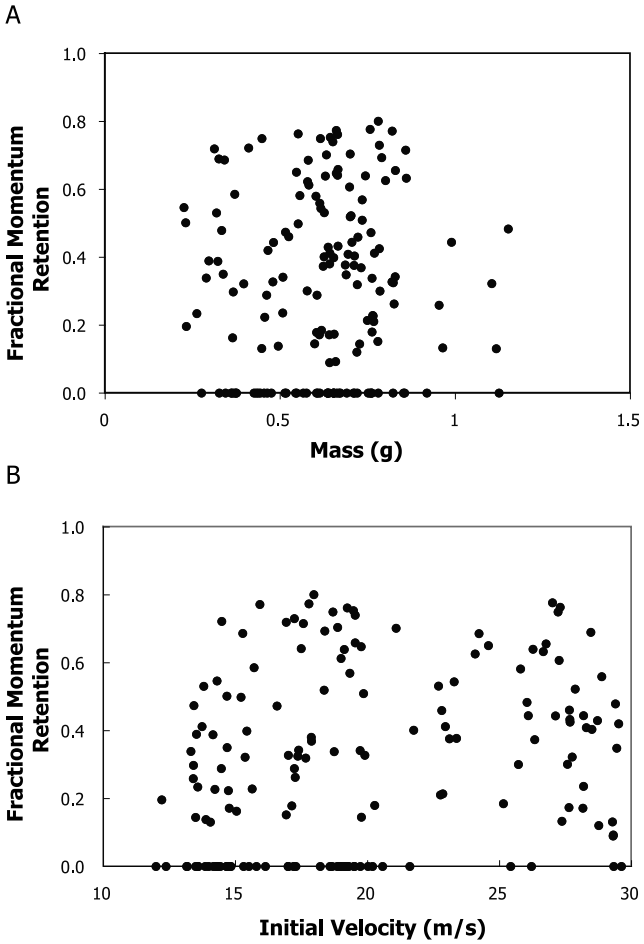

Figure 3. The fraction of momentum retained when a particle encounters a water substrate as (a) a function of particle mass and (b) initial velocity. A value of 0.0 denotes particles that did not rebound from the water surface. The momentum retained by the particles during particle-water interaction does not correlate with either its initial velocity or mass.

30 m/s. At velocities of 10 m/s, almost all particles sink when they impact water, so we focused our investigation on higher velocities. Additionally, there is likely only a very low percentage of particles in an over-water pyroclastic density current that travel an appreciable distance with a velocity at or less than 10 m/s [*Dufek and Bergantz*, 2007a]. We are limited to maximum velocity of 30 m/s by the maximum pressure of the compressed nitrogen, and safety concerns. High-energy pyroclastic density currents can likely produce flows that exceed these values [*Dufek and Bergantz*, 2007b; *Esposti Ongaro et al.*, 2008], but this covers a large range of average particle impact velocities at the base of flows. As examined later, the dynamics are much more sensitive to impact angle than velocity.

[9] In addition to varying the incoming velocity of the particles, we are able to vary the incoming angle by systematically changing the pitch angle (ϕ) of the launch tube. The lowest angle we could achieve is 10°. We limited experiments beyond a maximum angle of 30°, because our results show that above this angle very few particles bounce off the surface of the water.

[10] The pumice-substrate interaction was recorded at 500 frames per second with a Redlake high-speed video camera. The camera records images with a resolution of 1280 × 516 pixels, with a shutter speed of 1/2000 s. Using MIDAS video analysis software, we then determined the particle location at a given instant in time, with an accuracy of 1–2 mm in any direction. After a collision, a particle will often bounce in an oblique direction, with a different yaw angle (Ψ) than its initial value (Figure 2). To account for this, we have built a particle collector to determine yaw angle within roughly ±5°. We divide the velocity observed by the video camera by the cosine of this yaw angle to correct for our ability to only calculate directly the component of velocity that is projected into the camera's viewing plane.

3. Experimental Results

[11] The results of the water and pumice bed experiments are compiled in Figures 3–7. We analyze the results in terms of the fraction of linear momentum retained by the particles during the collision. The angular momentum changes associated with impacts were not measured, although it plays an important role in the gyroscopic stability for oblate particles, a phenomenon familiar to stone skipping enthusiasts [*Clanet et al.*, 2004]. As the particle's mass remains nearly constant following collision in most of the experiments [*Dufek and Manga*, 2008], the momentum retention fraction is effectively a restitution coefficient. However, we note that in the pumice bed experiments, sometimes the particle ejected from the bed is a different particle than the impacting particle.

[12] There is considerable scatter in both sets of experiments, primarily owing to the shape irregularity of the individual pumice particles and not to experimental error. This necessitated conducting numerous experiments to

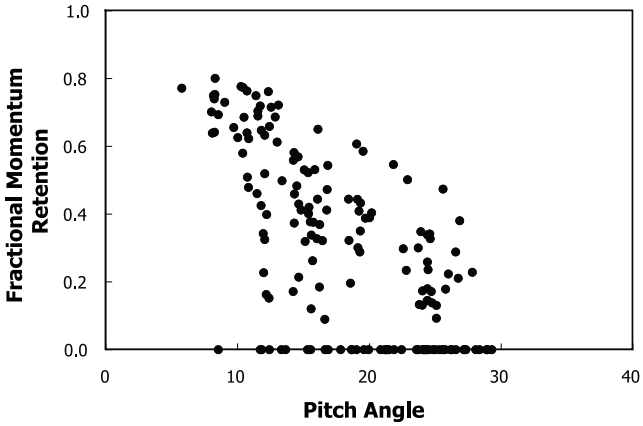

Figure 4. The fraction of momentum retained when a particle encounters a water substrate as a function of initial pitch angle. Shallow trajectory particles retain much more of their momentum than high-angle impacts. A least squares fit for the above set of data (excluding the zero momentum retained data) is $e = 0.83 - 0.029\phi$.

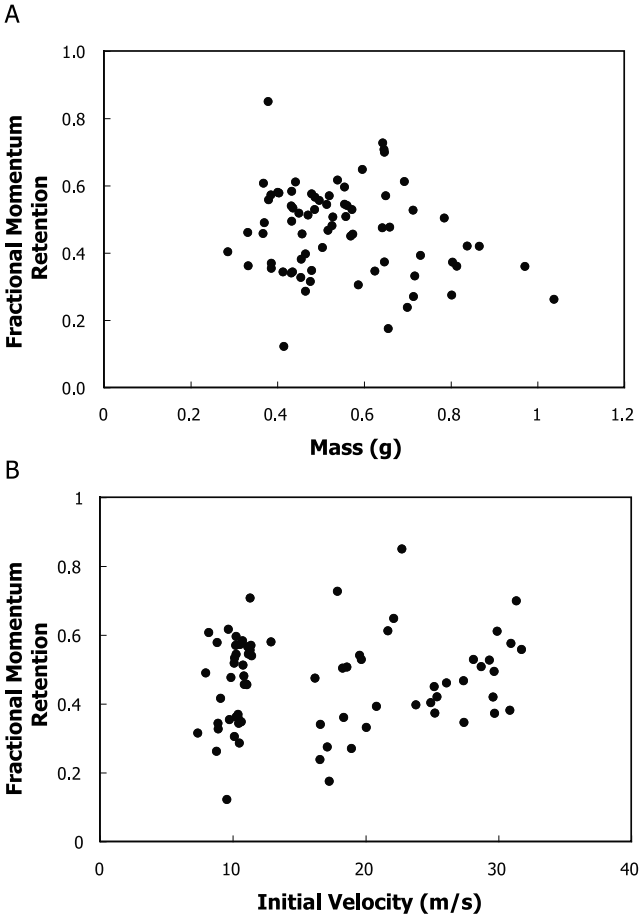

Figure 5. Fractional momentum retained when a particle encounters a bed of pumice of the same size as the impacting particle as a function of (a) particle mass and (b) initial velocity. There is no correlation between either the mass or velocity of the impactor and the fraction of momentum retained in the ejected particle with t test values of -1.8 and 1.1, respectively.

describe the mean and range of potential outcomes when particles interact with a boundary. As we used natural materials (pumice) in the experiments we would expect that this distribution of behavior would also occur in natural flows.

[13] In both the water and pumice bed experiments, t tests show that the fraction of momentum retained after the collision with the boundary is insensitive to particle velocity and the mass of the particle (Figures 3 and 5). However, the amount of momentum retained is correlated with the initial pitch angle. We performed a least squares fit to the data in Figure 4 and Figure 6 to describe the relationship with the pitch angle. For particles encountering a water surface the momentum retained is given by

$$e = 0.8343(\pm 0.042) - 0.0291(\pm 0.0024)\phi, \quad (1)$$

where e is the fraction of momentum retained, or effective restitution coefficient, and ϕ is the pitch angle from horizontal given in degrees.

[14] In this fit the particles that sank immediately were excluded. Their role is discussed separately below in determining a critical skipping condition for these pumice particles. For particles encountering a bed of pumice the amount of momentum retained is given by

$$e = 0.7307(\pm 0.044) - 0.0144(\pm 0.0023)\phi. \quad (2)$$

The amount of momentum retained, at a given pitch angle, is somewhat lower for particles rebounding from the collision with the pumice bed compared to water, likely due to the roughness of the pumice bed. However, in all cases involving the pumice bed, there were particles ejected, while a certain subset of particles immediately sank when interacting with water.

[15] Whether or not a particle rebounds or skips during a particle-water encounter depends on both the initial velocity and pitch angle (Figure 7). We again performed a least square fit of the results to determine the probability of sinking:

$$S = 9.3755 - 1.9452|V| + 3.1363\phi. \quad (3)$$

Here S is the percentage of particles that sink, $|V|$ is the speed of the particle, and ϕ is the pitch angle. S is restricted to positive values. The pitch angle and speed dependence of the sinking criteria is consistent with other studies examining the skipping of stones [*Clanet et al.*, 2004] and bouncing of military bombs during the Second World War [*Johnson*, 1998]. Spin can also play an important role in stabilizing the angle of attack of disk shaped objects, causing spherical bodies to skip at shallower angles if backspin is introduced. Due to particle shape irregularities, the experiments had a range of spins, and here we emphasize the probability of skipping rather than discussing a critical angle at a specific velocity for more idealized shapes. Based on analysis of lift and pressure [*Johnson*, 1998], the maximum angle for skipping for spherical, nonspinning particles is $\sim 23^\circ$ for the sizes and density of the pumice particles we used.

[16] The average fractional change in particle velocity when pumice encounters a bed of pumice, the effective restitution coefficient, can be estimated using these experiments. We compute this average restitution coefficient by

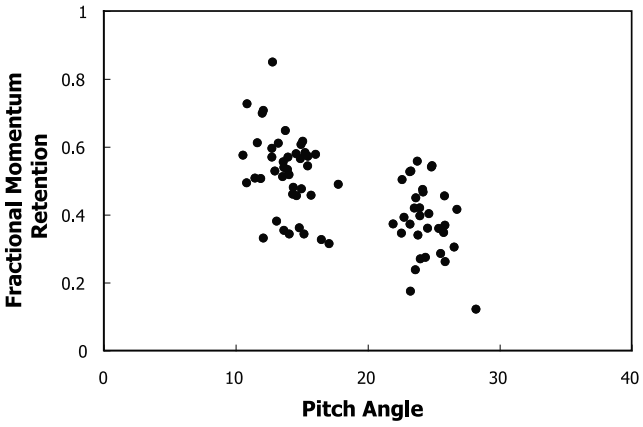

Figure 6. The fraction of momentum retained when a particle impacts a bed of pumice as a function of initial pitch angle.

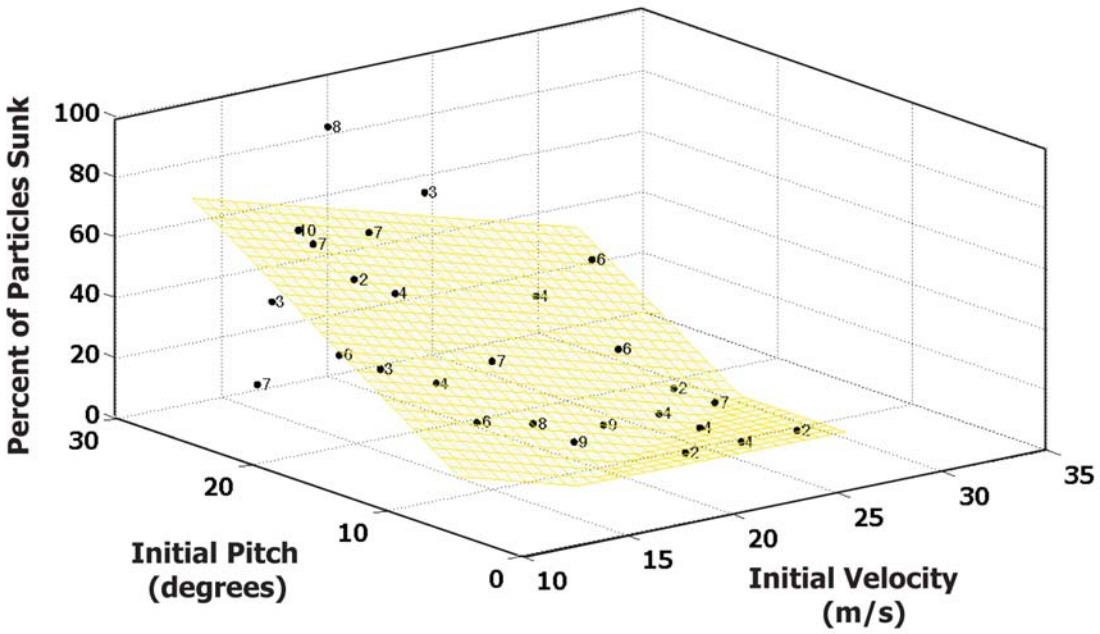

Figure 7. The percentage of particles that sink as a function of initial velocity and pitch angle. As denoted, shallow angle, high-velocity impacts were much more likely to rebound from the surface. Each point represents the mean in a given bin of velocity and pitch angle, and the number next to each point shows the number of data points taken for each average. The light shaded region denotes the plane fitting the data (equation (3)). The average error in the percentage of particles sinking with this fit is 9.86%.

integrating over all angles examined in the experiment and dividing by the range of angles. This results in an effective average restitution coefficient (e) of 0.51. We note that sometimes particles other than the original projectile are ejected from the bed, and so these measurements reflect a somewhat different process than is usually measured in single particle restitution coefficient experiments [*Cagnoli and Manga*, 2003]. However, for particles impacting a granular bed, common in many volcanic settings, we argue that these measurements are more appropriate, and we recommend this value for numerical and analytical models that consider particle-boundary interactions.

4. Clast Transport in Particle-Stratified Flow: Separating Particle Concentration and Boundary Effects

[17] We examine the role of particle-particle, particle-gas, and particle-boundary interaction in a suite of calculations in which these effects are completely uncoupled. In these calculations we hold the flow height and velocity constant, and introduce a test particle at the top of the flow. The test particle initially has the same velocity as the flow. We vary the particle concentration and the boundary conditions to reflect the experimentally determined relations for a pumice bed boundary and a water boundary. The full Lagrangian equation of motion for the particle is given as [*Burgisser and Bergantz*, 2002; *Dufek and Bergantz*, 2007a; *Fan et al.*, 2000]

$$\frac{du_{p,i}}{dt} = F_g + F_s + g_i\left(\frac{2\rho_p - 2\rho_g}{2\rho_p + \rho_g}\right)\delta_{i2}. \tag{4}$$

Here, and below, the subscripts p and g refer to particles and the gas phase, respectively, $u_{p,i}$ are the velocity vectors, ρ is density, δ_{i2} is the Kronecker delta operator (equals 1 for the vertical direction and 0 otherwise) and g_i is gravity. The F_g term is the drag force imparted by the gas, F_s is a force imparted through the collision of small particles, and the final term is the body force. Particle-gas interaction is described through a drag coefficient that depends on the particle Reynolds number. This is described as

$$F_g = \frac{f}{\tau_p}\left(u_{p,i} - u_{g,i}\right)\left(\frac{2\rho_p}{2\rho_p + \rho_g}\right), \tag{5}$$

where f is an empirical correction to the drag coefficient sensitive to particle Reynolds number:

$$f = 1 + 0.15\mathrm{Re}_p^{0.687} + \frac{0.0175}{1 + 42500\mathrm{Re}_p^{-1.16}}, \tag{6}$$

and τ_p is the particle response time (the characteristic time for a particle to accelerate to match the fluid velocity),

$$\tau_p = \frac{\left(\rho_p - \rho_g\right)d_p^2}{18\mu}. \tag{7}$$

[18] The particle Reynolds number (Re_p) is given as

$$\mathrm{Re}_p = \frac{\rho_g\left|u_{p,i} - u_{g,i}\right|d_p}{\mu}. \tag{8}$$

Table 1. Parameters Descriptions[a]

Parameters	Description	Units
$c_{P,m}$	heat capacity	J (kg K)$^{-1}$
d_p	particle diameter	M
e	restitution coefficient	
F_g	specific gas drag	m s^{-2}
F_s	specific particle-particle drag	m s^{-2}
g_0	radial distribution function	
H	mean interphase heat transfer	J (m^3 s)$^{-1}$
H	flow height	m
I	interphase momentum transfer (drag)	Pa m^{-3}
y'	nondimensional length	
m	mass	kg
P	pressure	Pa
q	thermal heat flux	J (m^2 s)$^{-1}$
S	percent of particles that sink	
T	temperature	K
u_i	velocity	m s^{-1}
$\|V\|$	speed	m s^{-1}
α	volume fraction	
$\alpha^{\max}$	close-packed particle volume fraction	
ϕ	pitch angle	deg
Ψ	yaw angle	deg
μ	viscosity	Pa s
ρ	density	kg m^{-3}
θ	granular temperature	m^2 s^{-2}
γ	particle concentration gradient	m^{-1}
τ_{ij}	stress tensor	Pa

[a]Subscript m refers to a general phase and can take on values 0, 1, 2, 3. Lagrangian phases are denoted by 0, 1 is the gas phase, 2 and 3 are particle Eulerian phases. The subscript p refers to Lagrangian particles (taking on the value 0), s refers to particle Eulerian particles (taking on values 2 and 3), and g refers to the gas phase 1. Subscripts i and j refer to spatial dimensions.

Further information about the symbols we use is summarized in Table 1. The force felt by a larger particle encountering numerous smaller particles is computed by determining the collisional frequency and the acceleration imparted by a single collision using kinetic theory. We further assume that the velocity distribution of the small particles can be described as Gaussian, i.e., by a mean velocity and a variance or granular temperature (θ) [*Dufek and Bergantz*, 2007a; *Fan et al.*, 2000; *Gidaspow*, 1994]. The result is

$$F_s = \left[\frac{6\alpha_2\sqrt{\theta}g_0(d_2+d_0)^2}{\sqrt{\pi}d_2^3}\right]\left[\frac{\rho_2 d_2^3(1+e)(u_{2,i}-u_{0,i})}{\rho_2 d_2^3+\rho_0 d_0^3}\right], \quad (9)$$

where the subscript 2 refers to a population of small particles (in these calculations we assume 10 μm particle diameters), and 0 refers to a single, larger particle. (We have reserved the subscript 1 for a later gas phase). We assume the restitution coefficient, e, has a value of 0.51 based on our earlier experiments, and for the purposes of the present calculation we assume that the granular temperature of the small particle population is 10% of the mean velocity of the particles. This generates a relatively coherent flow, and broadening of the distribution with a greater granular temperature would result in more numerous collisions and stronger particle-particle drag. The radial distribution function (a pair correlation function normalized by number density) at the distance of two touching particles (2 $\times$ particle radius) is approximated as

$$g_0 = \left[1-\left(\frac{\alpha_2}{\alpha_2^{\max}}\right)^{1/3}\right]^{-1}. \quad (10)$$

Under very dilute conditions g_0 is approximately one and increases as the close packing is approached. Most particle-laden gravity currents have vertical particle-concentration gradients, and here we assume that this gradient is linear from the top to the bottom of the flow. We define the particle volume fraction field as

$$\alpha_2 = \alpha_2^0\frac{y}{H}. \quad (11)$$

[19] We fix the height of the flow, H, and vary the basal particle concentration value, α_2^0, the basal particle concentration gradient, $\gamma = \alpha_2^0/y'$, the size of the large particle, d_0, and the nature of the boundary condition to either reflect a pumice bed boundary or water boundary. The vertical length scale y' is normalized by the flow height H, and the horizontal length scale x' is normalized by the distance the particle travels under only the influence of aerodyanamic drag. Some sample trajectories for pumice bed and water boundaries with different particle concentration gradients are shown in Figure 8. These calculations are terminated when the maximum vertical height achieved after rebounding from the boundary is less than the radius of the particle. We note that these calculations do not include terms for rolling along the surface, which could potentially extend the runout distance for the pumice boundary case.

[20] Large clasts are most sensitive to varying boundary conditions when the particle concentration is small. When these particles impact the boundary they typically saltate along the surface in both the water and pumice bed boundary cases, although the specific distance they saltate is sensitive to the velocity and trajectory of their impact (both of which are a function of particle size), and the drag forces encountered near the boundary. In the extreme case when no fine particles are present to exert a particle-particle drag force, a test particle with a radius of 0.02 m that descends through a 100 m flow traveling at 80 m/s (Figure 8), travels ~50% further due to saltation on a pumice bed than would be expected if it immediately sedimented upon first reaching the boundary. Skipping along the water surface also increases the distance ~30% for the same conditions.

[21] Large clasts in dense flows, such as the example in Figure 8 that has a maximum volume fraction of 0.4, are relatively insensitive to boundary conditions. Again, here we specifically do not consider the potential feedback between fine particle concentration and the boundary, which can have important secondary effects if the particle concentration field is modified by the boundary. We consider such feedbacks in section 5 using a multiphase flow model. If the particle concentration is unaffected by the boundary this example shows that the transport distances for the two different boundary conditions are virtually indistinguishable. This occurs for two reasons, both related to the enhanced drag caused by particle collisions. First, the high particle concentration encountered at the base of the flow greatly increases the frequency of particle collisions that exerts a drag force given by equation (9). This slows the large particles during their descent. While this allows the particles to travel further in the flow, they have very little vertical velocity upon impact. This low vertical impact velocity results in low velocities following the impact (reduced from the impact velocity

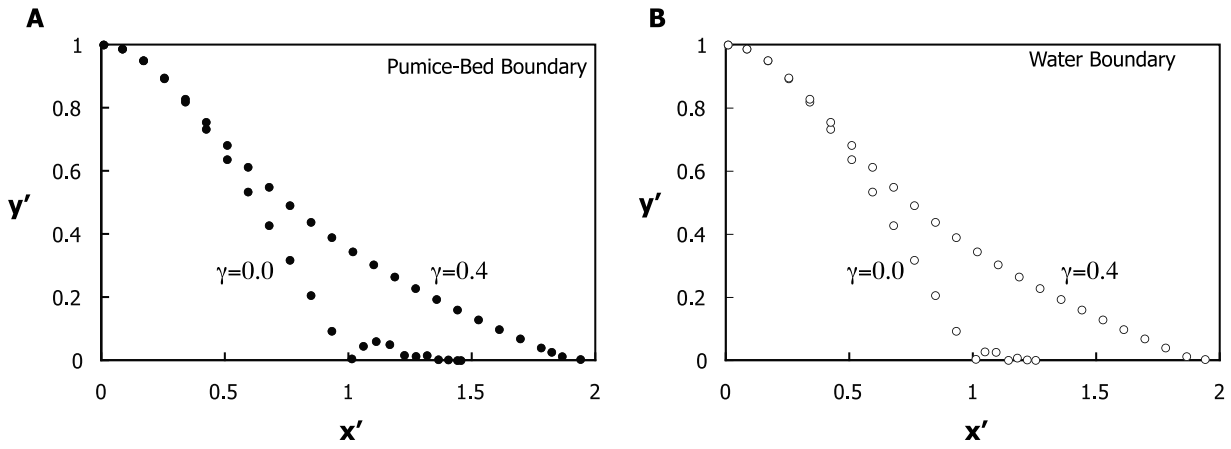

Figure 8. Example trajectories of a particle descending through a fine-particle flow, with two different concentration gradients ($\gamma = 0.0$ and $\gamma = 0.4$), and with (a) a pumice bed boundary and (b) water boundary condition. In these calculations, the "test" particle is 0.02 m in radius with a density of 1000 kg/m^3. The vertical length scale y' is normalized by the flow height H, and the horizontal length scale x' is normalized by the distance the particle travels under only the influence of aerodynamic drag. The maximum particle volume fraction that the particles encounter is indicated next to the trajectories. The particle positions are shown every 0.5 s, but in the calculations the computation is updated every 0.01 s to insure accurate detection of the collision with the boundary and to update the local concentration field experienced by the particle.

proportional to the restitution coefficient), and short distances traveled between successive, energy-dissipating impacts. Second, high particle concentration results in strong opposing forces as the particles begin to rebound from the surface. Since the rebound velocities are already small, the particle rapidly decelerates. For relatively large clasts such as the 2 cm radius particles considered here, the collision-cross section is large, and the drag force in particle enriched flows essentially traps the clasts at the interface where they can sediment. Again, if rolling or frictional interactions were included in this parameterization greater distances might be expected for the pumice boundary case, but not for the water boundary.

[22] A summary of the distance traveled due to boundary interactions and particle-particle interactions is shown in Figure 9 for a range of particle sizes and concentration gradients. In this plot the contours represent the scaled distance traveled normalized by the distance traveled by a particle only experiencing aerodynamic drag, a quantity we refer to as the "excess" distance. Also shown is the Stokes number (St) for a given particle radius, which represents the ratio between the particle aerodynamic response timescale (equation (7)) to the fluid timescale which we define here as the flow height divided by the flow velocity:

$$St = \frac{\tau_p}{\tau_f}. \tag{12}$$

[23] Figure 9 further emphasizes the insensitivity to the different boundary conditions when the fine particle concentration is high. Relatively small particles (between 0.001 and 0.01 m) at high particle concentrations can be transported more than 10 times what one would expect from a single particle initially traveling at the same velocity in a high-speed, gas-only, wind. At low, fine-particle concentrations, large clast transport becomes sensitive to the nature of the boundary conditions, with particles greater than ~0.01 m diameter beginning to have significantly different transport distances depending on whether a pumice bed or water boundary is considered.

5. Clast Transport in Dilute and Dense Flows: Multiphase Modeling

[24] Although it is instructive to treat the concentration of fine particles and the boundary conditions as uncoupled, as in section 4, previous work has indicated that flow runout and particle concentration are sensitive to boundary conditions [*Dufek and Bergantz*, 2007b]. Here we describe the use of an Eulerian-Eulerian-Lagranian (EEL) multiphase model to understand the transport of large clasts that are reactive to a locally evolving particle concentration field that is, in turn, responsive to boundary conditions. For the fine particles, in these calculations 10 μm, we make the assumption that during over-water transport any particle that reaches the base of the flows is lost from the flow. For particles <1 mm surface tension likely dominates over particle inertia, and should be more efficient at removing the particles from the flow. To implement this condition, we use the perfectly leaky boundary condition derived by *Dufek and Bergantz* [2007b] that used kinetic theory to calculate the collisional probability for particles reaching the bottom boundary in a given time increment. For ash-sized particles interacting with a solid, pumice bed boundary we use a modified *Johnson and Jackson* [1987] style boundary where particles lose a fraction of energy per particle-boundary interaction specified by a restitution coefficient. We assume that the average restitution coefficient for the ash particles is the same as the experimentally derived restitution coefficient for pumice particles. Here we assume that the roughness length scale of the boundary is larger than the small particle diameter, so that the boundary is effectively flat

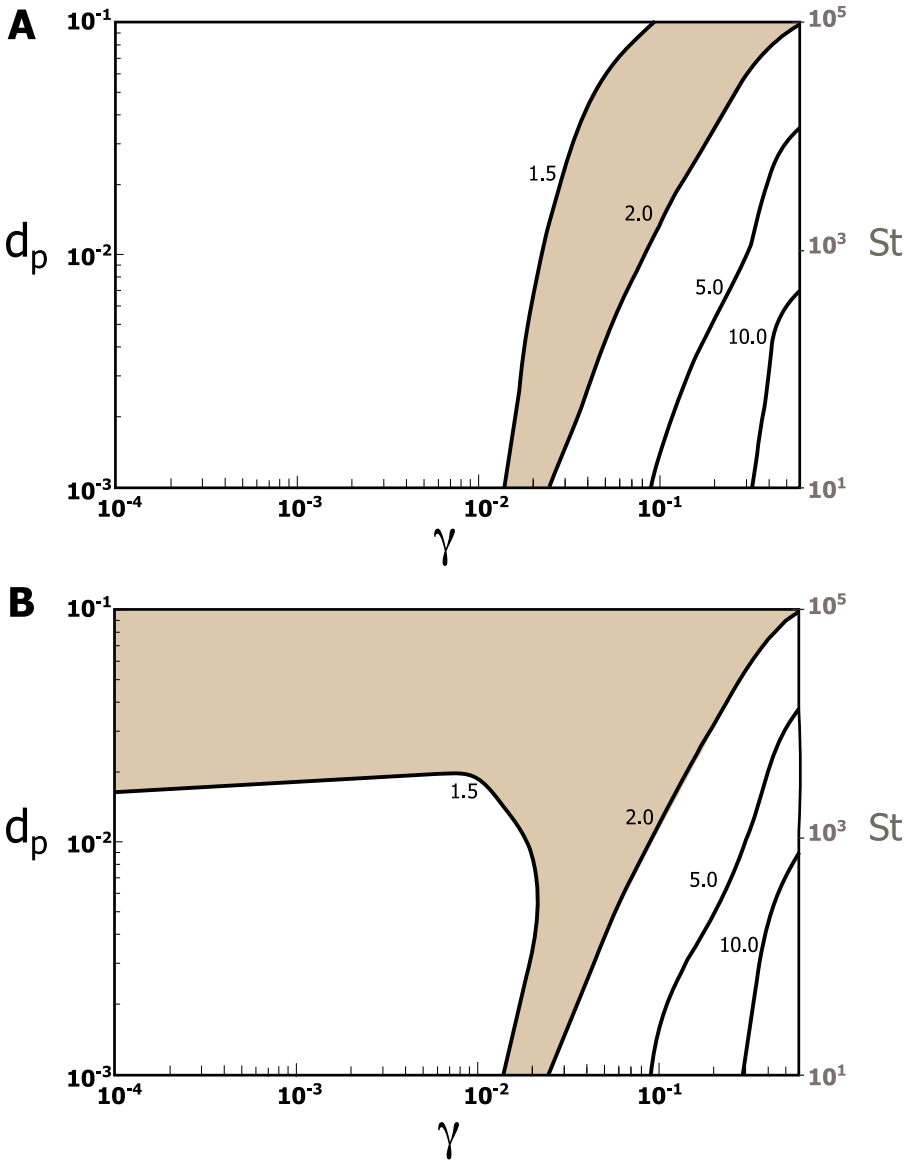

Figure 9. Contours of dimensionless excess distance traveled as a function of particle concentration gradient (γ) and particle diameter (d_p). (a) The experimentally determined water boundary conditions and (b) the pumice bed conditions. The regions between contours 1.5 and 2 have been shaded to emphasize the differences between the two boundary conditions. Large particles in dilute conditions travel further with pumice bed boundaries than their water boundary counterparts. In dense flows, individual particles are insensitive to the direct interaction of boundary conditions. Indirect particle-boundary interactions (changing particle concentration in response to boundaries) are not included in these calculations.

as far as the fine particles are concerned. More information on these boundary conditions is given by *Dufek and Bergantz* [2007b].

[25] We incorporated both leaky and saltation boundary conditions into continuum multiphase numerical simulations, based on the MFIX (multiphase flow with interphase exchanges) approach adapted for volcanic flows [*Dufek and Bergantz*, 2005; *Gera et al.*, 2004; *Syamlal et al.*, 1993]. In this and other similar continuum multiphase numerical approaches applied to volcanic conditions [*Clarke et al.*, 2002; *Dartevelle et al.*, 2004; *Dufek and Bergantz*, 2005; *Neri et al.*, 2002; *Todesco et al.*, 2006], separate continua (gas and particle) equations for mass, momentum and energy conservation are used to describe the physical system. We summarize the continua equations below. The gas and particle continuity equations are given as

$$\frac{\partial}{\partial t}\left(\alpha_g \rho_g\right) + \frac{\partial}{\partial \boldsymbol{x}_i}\left(\alpha_g \rho_g u_{g,i}\right) = 0 \tag{13}$$

and

$$\frac{\partial}{\partial t}\left(\alpha_s \rho_s\right) + \frac{\partial}{\partial \boldsymbol{x}_i}\left(\alpha_s \rho_s u_{s,i}\right) = 0, \tag{14}$$

respectively. Similarly, the momentum equations for the gas and particle phases are given as

$$\frac{\partial}{\partial t}\left(\alpha_g \rho_g u_{g,i}\right) + \frac{\partial}{\partial \boldsymbol{x}_i}\left(\alpha_g \rho_g u_{g,i} u_{g,j}\right) = \frac{\partial P_g}{\partial x_i}\delta_{ij} + \frac{\partial \tau_{g,ij}}{\partial x_j} + I_i + \alpha_g \rho_g g_i \tag{15}$$

and

$$\frac{\partial}{\partial t}\left(\alpha_s \rho_s u_{s,i}\right) + \frac{\partial}{\partial \boldsymbol{x}_i}\left(\alpha_s \rho_s u_{s,i} u_{s,j}\right) = \frac{\partial P_s}{\partial x_i}\delta_{ij} + \frac{\partial \tau_{s,ij}}{\partial x_j} - I_i + \alpha_s \rho_s g_i. \tag{16}$$

The gas and particle phase thermal energy conservation relations are

$$\alpha_g \rho_g c_{\mathrm{P},g}\left(\frac{\partial T_g}{\partial t} + u_{g,i}\frac{\partial T_g}{\partial \boldsymbol{x}_i}\right) = \frac{\partial q_g}{\partial x_i} - \overline{H}_{gs} \tag{17}$$

and

$$\alpha_s \rho_s c_{\mathrm{P},s}\left(\frac{\partial T_s}{\partial t} + u_{s,i}\frac{\partial T_s}{\partial \boldsymbol{x}_i}\right) = \frac{\partial q_s}{\partial \boldsymbol{x}_i} + \overline{H}_{gs}. \tag{18}$$

[26] Here α, ρ, and u_i are the volume fraction, density and velocity components, respectively. Pressure is denoted by P and the stress tensor is given by τ_{ij}. Heat capacity is given by c_p, temperature as T, and heat flux by q. Momentum exchange due to drag is given by I_i, and thermal exchange between phases is given by the $\overline{H}$ terms. A summary of the symbols used in these equations is included in Table 1. Constitutive relations required to close the momentum and thermal energy equations are described in detail by *Dufek and Bergantz* [2007b] and are given in the auxiliary material.[1] For collisional transfer of momentum, the constitutive relation for the particle phase is provided by kinetic theory similar to that used in the estimation of gas viscosities from molecular collisions [*Dufek and Bergantz*, 2005; *Lun et al.*, 1984]. This constitutive relation assumes binary, inelastic particle collisions. The collision rate and stress in the granular material depend on the fluctuating particle velocity. A separate transport equation for pseudothermal energy is solved in order to determine the granular temperature (variance of the velocity distribution) and close the granular stress in dilute conditions. Pseudothermal energy is assumed to be advected by the mean flow and diffuses along gradients in the granular temperature. Locally pseudothermal energy is produced by shear and by the relative velocity between the particle and gas phases [*Agrawal et al.*, 2001; *Benyahia et al.*, 2005] and is dissipated by inelastic collisions and by viscous damping in the carrier fluid. The production of fluctuating motions by gas-particle slip and dissipation by viscous forces ensures that the granular pseudothermal energy equation is coupled to the carrier fluid. At higher particle volume fractions, protracted frictional interaction of particles occurs and the frictional and collisional stresses are assumed to be additive [*Benyahia*, 2008; *Savage*, 1998; *Srivastava and Sundaresan*, 2003; *Syamlal*, 1987]. The frictional stress is developed using the postulate of a yield function and an associated flow rule to relate stress and strain rate, and has been adopted from theories of soil mechanics. The solids pressure in the frictional regime allows the solid phases to have some compressibility, but provides a resisting force to prevent unphysical void fractions. In the limit of volume fractions approaching the minimum void fraction both the frictional pressure and granular shear viscosity approach infinity, which prevents further circulation of material.

[27] The Lagrangian particles are coupled with the gas and particle continua through drag terms using an approach proposed by *Fan et al.* [2000]. In this Eulerian-Eulerian-Lagrangian (EEL) approach the Lagrangian particles are one-way coupled to both the particulate (solid) continua and the gas continua. Equation (4) gives the Lagrangian equation of motion that can be used to examine the trajectory of large, but volumetrically insignificant, particles in the flow. This equation is coupled to the gas phase continuum through the gas drag force (F_g) term and through the average effect of numerous collisions with small particles through the (F_s) term. When the Lagrangian particles reach the bottom boundary, the experimentally determined conditions are applied for either pumice bed flows or water-traversing flows.

[28] In the multiphase calculations, two particle sizes are considered with the continuum approach, those whose diameter is 10 μm and compose 95% of the flow, and 0.5 mm particles that comprise 5% of the flow. These particles have densities of 1000 kg/m^3 and have Stokes numbers of $\sim 4.0 \times 10^{-4}$ and ~ 1.0, respectively. Similar to the calculations in section 4, the flows are introduced into a two-dimensional domain at the left and are 100 m high and have velocities of 80 m/s. The gas and particles in the flow are initially 700 K and the ambient atmosphere is 300 K. We neglect subgrid-scale steam generation [*Dufek et al.*, 2007] for the over-water case. Density of the gas phase is computed using the ideal gas relation. To facilitate comparison to previous calculations made by *Dufek and Bergantz* [2007b], we normalize the horizontal distance by a length scale at which half the particles in the flow would have been sedimented, if the only force acting on the particles is gravitational settling. Horizontal resolution is 6.0 m and vertical resolution is refined at the base, varying from 1.0 to 6.0 m.

[29] We consider four simulated conditions. For both the water and pumice bed boundaries we simulate two different initial volume fractions of particles: one with an initial particle concentration is 0.025 and one in which the particle concentration is 0.40. Lagrangian particles are introduced throughout the flow duration near the flow inlet and their grain size distribution is from 1 μm to 10 m, with a uniform deviate distribution. In all cases, the saltating boundaries result in further runout distance for the small particles relative to the leaky boundaries for the small particles. As explained previously, this results primarily from the enhanced energy dissipation when particles are removed from the flow [*Dufek and Bergantz*, 2007b]. Saltating small particles lose only a fraction of their energy per boundary interaction, not all their energy, and thus retain more energy per time than leaky flows. We stress that these flows contain no topography that could modify this assessment.

[1] Auxiliary materials are available in the HTML. doi:10.1029/2008JB006216.

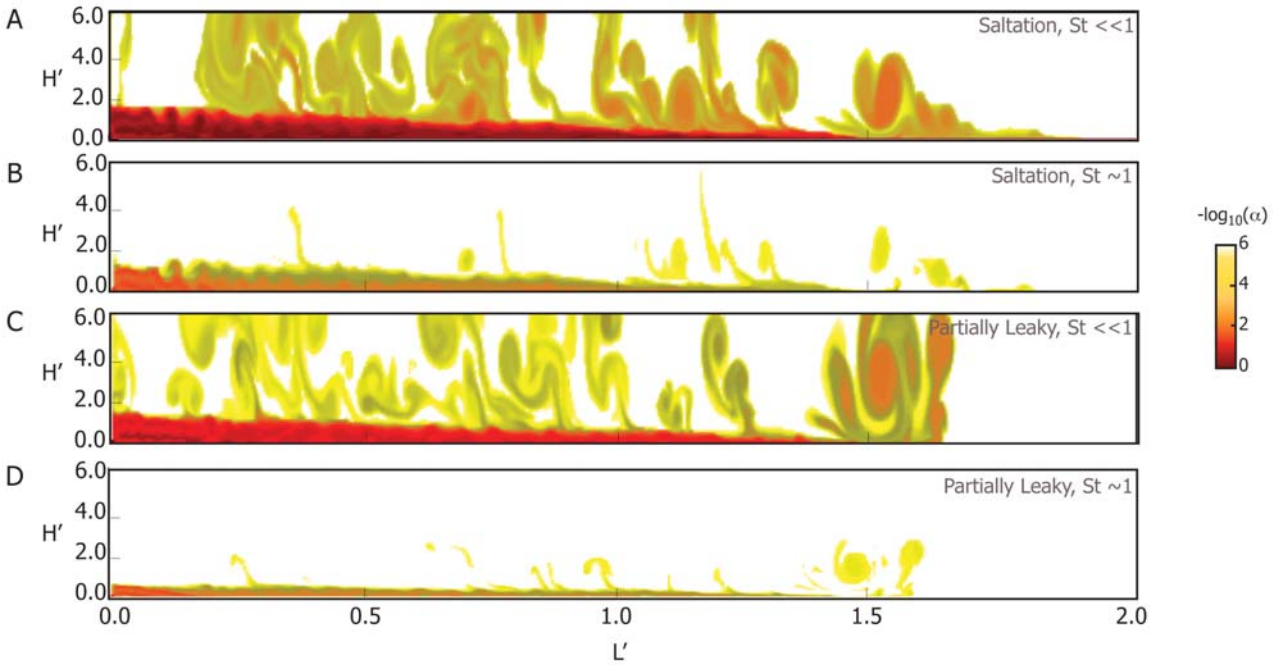

Figure 10. Multiphase simulation using two different boundary conditions. (a and b) The pumice bed boundaries for two particle sizes (St $\ll$ 1 and St $\sim$ 1). (c and d) Leaky boundary conditions. In both cases the particle velocity probability distribution is integrated to determine the number of impacts that occur at the bed during a time step, and how much momentum is dissipated during the encounter. Pumice bed or saltation boundary flows continue to propagate further than the leaky flow counterparts, given the absence of topography in the simulations.

[30] An example of the particle concentration field is shown in Figure 10. In both the leaky flows and saltating flows, particle concentration gradients develop during transport. With the saltating boundary conditions, a bed load region of enhanced concentration develops as particles remain mobilized in the flow after interacting with the bottom boundary.

[31] The Lagrangian particles are sensitive to the development of regions of high particle concentration as would be expected from equation (4) and are also segregated in regions of dominant vortical motion (Figure 11). Most of the particles with Stokes numbers greater than 1000 ($\sim$1 cm in diameter in these simulations) rapidly sediment from the flows that are initially dilute (volume fraction 0.025).

[32] Likewise, the initially dense flows (volume fraction 0.40) that traverse water fail to produce a concentrated bed load region, and also do not to preferentially transport particles with Stokes number in excess of 1000 much further than the dilute flows ($\sim$20% further), although they do have longer runout and transport smaller particles further than in the dilute case. However, the pumice bed, dense flows, transport large clasts considerably further due to their higher particle concentration gradients (Figure 11). The saltating boundary condition enables the initially dense flows to remain much denser than their leaky flow counterparts that rapidly lose particles through the bottom boundary. Compared to the initially dense, over-water flow, the maximum distance of St > 1000 particles is over 350% further in the pumice bed case.

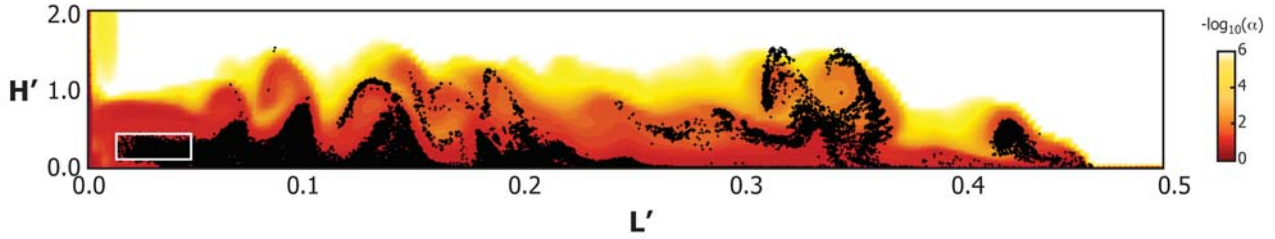

Figure 11. Coupled Eulerian-Eulerian-Lagrangian (EEL) simulation for the pumice bed boundary conditions. Lagrangian particles are seeded into the flow from the region outlined by the white box and are shown as black dots in the figure. The colored background denotes the particle volume fraction from the continuum or Eulerian portion of the simulations using the same color bar as in Figure 9. The Lagrangian particle size distribution is uniform deviate and sizes range from 1 μm to 10 m.

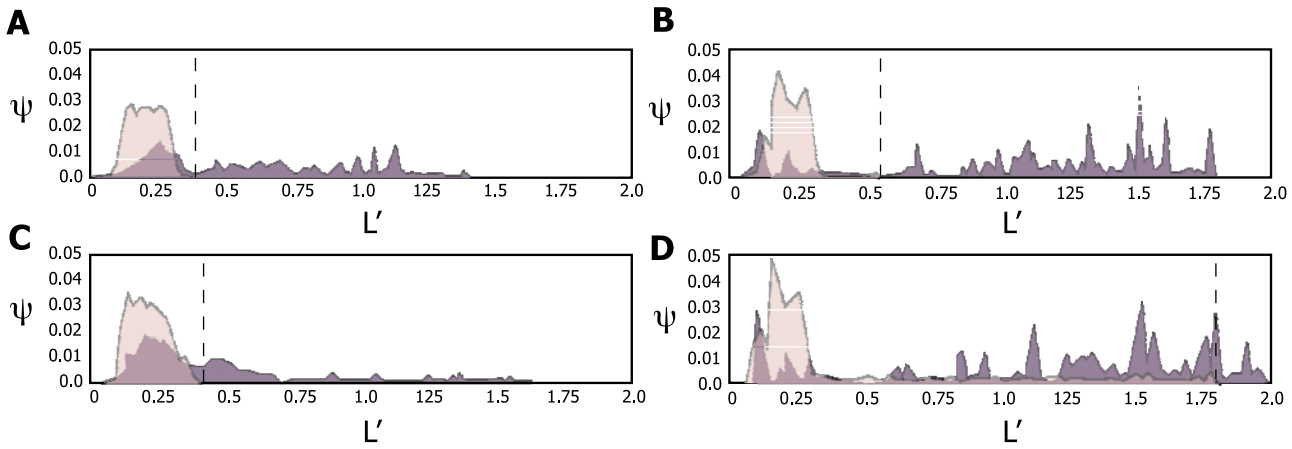

Figure 12. Final distribution of Lagrangian particles; the fraction of particles (ψ) in a size range is plotted versus the nondimensional transport distance. The light shaded region depicts particles greater than St = 1000 (~1 cm), while the dark shaded regions are for particle less than St = 1000. The dashed line shows the furthest extent of the St > 1000 particles. The four conditions shown are (a) Leaky boundary, initial particle volume fraction of 0.025; (b) pumice bed boundary, initial particle volume fraction of 0.025; (c) leaky boundary, initial particle volume fraction of 0.40; and (d) pumice bed boundary, initial volume fraction of 0.40. Only with the pumice bed boundary condition and elevated particle volume fraction are some St > 1000 particles transported for nearly the entire runout of the flow.

[33] Again, the enhanced transport distance is not directly due to the enhanced skipping of particles along the bottom boundary. While this has some influence, the differences are quite modest as is evidenced by the only slight variation in the water and pumice-traversing flows in dilute conditions (Figures 12a and 12c). The collisions with fine particles, especially in the bed load region, appear to be responsible for the energy transfer necessary for the greatly enhanced transport of these particles.

6. Sensitivity of Pyroclastic Density Currents to Bed Conditions

[34] The inference of dilution and rapid loss of large clasts from flows traversing water appears consistent with many observations of pyroclastic flow deposits that have traversed large bodies of water such as the Koya ignimbrite [*Ui*, 1973], flows from Krakatau [*Carey et al.*, 1996; *Mandeville et al.*, 1996], flows from Okmok [*Burgisser*, 2005], and the early flows from the Kos Plateau Tuff [*Allen et al.*, 1999]. In the case of the Krakatau eruption, eyewitness accounts and on-land deposits demonstrate that the flows traveled over water for over 80 km, but were missing larger clasts present in proximal submarine deposits [*Carey et al.*, 1996; *Mandeville et al.*, 1996]. Flows from the Okmok (2050 years B.P.) eruption that reached the neighboring island of Unalaska were significantly finer than deposits of flows before reaching the sea. The Koya ignimbrite, while far-reaching, was very thin and fine-grained after traversing water. The bifurcation of flows upon reaching the sea, where the bed load forms submarine currents and the suspended load remains above the water surface has been noted in previous experiments [*Freundt*, 2003]and simulations [*Dufek and Bergantz*, 2007a, 2007b; *Dufek et al.*, 2007] and is in general agreement with these observations.

[35] The early flows of the voluminous Kos Plateau Tuff (>100 km^3 dense rock equivalent of rhyolite) that were inferred to traverse water to the south of the eruptive center were finer than inferred over-land deposits to the north [*Allen and Cas*, 2001] fitting the general model of over-water transport. However, later and climatic, pyroclastic density currents from this eruption had maximum grain sizes that were similar between over-water and over-land transport at similar radial distances from the source, confounding the general over-water fining interpretation. Topographic differences almost certainly played a role in the northward versus southward flows [*Branney and Kokelaar*, 1997], but it is more difficult to attribute temporal changes to the flow based on topographic control. While the active tectonics of the region have led to different interpretations of sea level at the time of the eruption (161 kyr) [*Allen and Cas*, 2001; *Pe-Piper et al.*, 2005], the differences in the early units do suggest that at least a shallow sea existed to the south of the Kos caldera while to the north land was subaerially exposed. Three-dimensional simulations of the Kos eruption using completely leaky and saltating boundaries, including topographic effects, reproduced the spatial pattern of the maximum grain sizes from the early units of the eruption, but a completely leaky boundary could not explain the large clasts that were transported over 20 km from the source over a putative water-filled basin (some over 10 cm in diameter) [*Dufek and Bergantz*, 2007a]. Ballistic trajectories for these distances and clast sizes are not feasible, and nearly omnipresent andesite lithic clasts from this eruption are almost certainly from erosion near the eruptive source as the flows crossed either water, limestone, or soft sediments to reach the locations on the island of Tilos or the Turkish peninsula of Datca. On this basis, *Dufek and Bergantz* [2007a] suggest that the differences between the early and late units of the eruption (and between the late unit and other water-traversing flows) were due to one of the following factors: (1) the voluminous size of the eruption generated very different dynamics that enabled the transport of large clasts in a way that does not scale with other over-water pyroclastic density currents; (2) the bounc-

ing of clasts from the water surface can account for the enhanced transport of the lithics; (3) a pumice raft formed and enabled saltation. The numerical simulations, using the eruptive flux inferred from the Kos eruption that reproduces the deposit distribution and flow regime (collapsing column), did not produce the enhanced transport and so factor 1 seems unlikely. Also, although the first units of the eruption were smaller, the inferred eruptive flux was likely within an order of magnitude of the climax of the eruption, making vast disparities in the clast transport less likely [*Allen*, 2001]. In this paper we developed a model for the skipping of large particles along the water surface and showed that under certain circumstances this could increase lithic transport by 50%. However, this effect is not sufficient to explain the enhanced transport of lithics in the Kos Plateau Tuff [*Dufek and Bergantz*, 2007a].

[36] Of these possibilities, the enhanced transport by the formation of the pumice raft appears to be most plausible, especially given that the pumice would have cooled substantially during transport, and at the time of the climatic eruption several meters of rafted material could have existed at the surface of the sea [*Allen et al.*, 1999; *Dufek and Bergantz*, 2007a]. Most Kos pumice has a density less than that of seawater, and pumice less than $\sim$200°C ingests water on minutes to year timescales [*Dufek et al.*, 2007; *Whitham and Sparks*, 1986], enabling a raft to presumably last during the inferred hours to days of the climatic part of Kos eruption.

[37] Such a pumice raft would likely behave much like the pumice bed boundary condition examined here. Previously, *Dufek and Bergantz* [2007a] suggested that the direct effect of saltating along the pumice raft might account for increased distance, and our experiments do show a modest increase in distance transported due to this effect (tens of percent further distance transported). However, the more pronounced effect of the formation of a pumice raft is the development of a particle-enriched bed load in which high concentrations of fine particles can develop in the near-bed region. These particles have much greater residence times than large particles considered in isolation, and our work here suggests that energy transfer from fine particles to larger clasts can enhance large clast transport by an order of magnitude greater than the enhanced saltation promoted by the pumice bed boundary. As fine particles can be mobilized in a flow through a variety of effects including gas pore pressure fluidization [*Druitt et al.*, 2007; *Druitt et al.*, 2004; *Girolami et al.*, 2008; *Roche et al.*, 2006], entrainment [*Bursik and Woods*, 1996; *Choux and Druitt*, 2002; *Dufek et al.*, 2007], and collisional and frictional interaction in a bed load region [*Dellino et al.*, 2007; *Dufek and Bergantz*, 2007b], the energy transfer from fine particles to larger particles is likely pervasive in most flows. Additionally, the in situ production of ash through comminution during the transport of these flows provides additional fines that can enhance the transport of less comminuted large clasts [*Dufek and Manga*, 2008; *Rose et al.*, 2008].

7. Conclusions

[38] In this investigation we performed experiments on the momentum dissipated when particles encounter pumice bed and water substrates. While, all else being equal, high Stokes number particles will saltate more efficiently on pumice bed substrates, the differences can be modest. However, both a simplified and multiphase model demonstrate that large clast transport can be greatly enhanced by the transfer of momentum from fine particles, such as ash, to the larger clasts. In this way, impermeable boundaries, such as a pumice bed, primarily influence large clast transport not through direct interaction, but by maintaining a particle-rich bed load region that enhances the interaction between small particles and large clasts. Such interactions are likely common in the transport of large lithic clasts that are nearly ubiquitous in ignimbrites.

[39] **Acknowledgments.** This work was supported by NSF grants 0809321 (J.D.) and 0809564 (M.M) and the Miller Institute for Basic Research in Science. We thank Louis Giersch for discussions on experimental design and the reviewers for helpful suggestions.

References

Agrawal, K., P. N. Loezos, M. Syamlal, and S. Sundaresan (2001), The role of meso-scale structures in rapid gas-solid flows, *J. Fluid Mech.*, *445*, 151–185, doi:10.1017/S0022112001005663.

Allen, S. R. (2001), Reconstruction of a major caldera-forming eruption from pyroclastic deposit characteristics: Kos Plateau Tuff, eastern Aegean Sea, *J. Volcanol. Geotherm. Res.*, *105*, 141–162, doi:10.1016/S0377-0273(00)00222-5.

Allen, S. R., and R. A. F. Cas (2001), Transport of pyroclastic flows across the sea during explosive, rhyolitic eruption of the Kos Plateau Tuff, Greece, *Bull. Volcanol.*, *62*, 441–456, doi:10.1007/s004450000107.

Allen, S. R., E. Stadlbauer, and J. Keller (1999), Stratigraphy of the Kos Plateau Tuff: Product of a major Quaternary explosive rhyolitic eruption in the eastern Aegean, Greece, *Int. J. Earth Sci.*, *88*, 132–156, doi:10.1007/s005310050251.

Benyahia, S. (2008), Validation of two continuum granular flow theories, *Ind. Eng. Chem. Res.*, *47*, 8926–8932, doi:10.1021/ie8003557.

Benyahia, S., M. Syamlal, and T. J. O'Brien (2005), Evaluation of boundary conditions used to model dilute, turbulent gas/solids flows in a pipe, *Powder Technol.*, *156*, 62–72, doi:10.1016/j.powtec.2005.04.002.

Branney, M. J., and P. Kokelaar (1997), Giant bed from a sustained catastrophic density current flowing over topography: Acatlan ignimbrite, Mexico, *Geology*, *25*, 115–118, doi:10.1130/0091-7613(1997)025<0115:GBFASC>2.3.CO;2.

Branney, M. J., and P. Kokelaar (2002), Pyroclastic density currents and the sedimentation of ignimbrites, *Mem. Geol. Soc.*, *26*, 8 pp.

Burgisser, A. (2005), Physical volcanology of the 2050 BP caldera-forming eruption of Okmok Volcano, Alaska, *Bull. Volcanol.*, *67*, 497–525, doi:10.1007/s00445-004-0391-5.

Burgisser, A., and G. W. Bergantz (2002), Reconciling pyroclastic flow and surge: The multiphase physics of pyroclastic density currents, *Earth Planet. Sci. Lett.*, *202*, 405–418, doi:10.1016/S0012-821X(02)00789-6.

Bursik, M., and A. Woods (1996), The dynamics and thermodynamics of large ash flows, *Bull. Volcanol.*, *58*, 175–193, doi:10.1007/s004450050134.

Cagnoli, B., and M. Magna (2005), Vertical segregation in granular mass flows: A shear cell study, *Geophys. Res. Lett.*, *32*, L10402, doi:10.1029/2005GL023165.

Cagnoli, B., and M. Manga (2003), Pumice-pumice collisions and the effect of the impact angle, *Geophys. Res. Lett.*, *30*(12), 1636, doi:10.1029/2003GL017421.

Carey, S., H. Sigurdsson, C. Mandeville, and S. Bronto (1996), Pyroclastic flows and surges over water: An example from the 1883 Krakatau eruption, *Bull. Volcanol.*, *57*, 493–511, doi:10.1007/BF00304435.

Choux, C. M., and T. H. Druitt (2002), Analogue study of particle segregation in pyroclastic density currents, with implications for the emplacement mechanisms of large ignimbrites, *Sedimentology*, *49*, 907–928, doi:10.1046/j.1365-3091.2002.00481.x.

Clanet, C., F. Hersen, and L. Bocquet (2004), Secrets of successful stone-skipping, *Nature*, *427*, 29, doi:10.1038/427029a.

Clarke, A. B., B. Voight, A. Neri, and G. Macedonio (2002), Transient dynamics of vulcanian explosions and column collapse, *Nature*, *415*, 897–901, doi:10.1038/415897a.

Dartevelle, S., W. I. Rose, J. Stix, K. Kelfoun, and J. W. Vallance (2004), Numerical modeling of geophysical granular flows: 2. Computer simulations of Plinian clouds and pyroclastic flows and surges, *Geochem. Geophys. Geosyst.*, *5*, Q08004, doi:10.1029/2003GC000637.

Dellino, P., B. Zimanowski, R. Buttner, L. La Volpe, D. Mele, and R. Sulpizio (2007), Large-scale experiments on the mechanics of pyr-

oclastic flows: Design, engineering, and final results, *J. Geophys. Res.*, *112*, B04202, doi:10.1029/2006JB004313.

Druitt, T. H., G. Bruni, P. Lettieri, and J. G. Yates (2004), The fluidization of ignimbrite at high temperature and with mechanical agitation, *Geophys. Res. Lett.*, *31*, L02604, doi:10.1029/2003GL018593.

Druitt, T. H., G. Avard, G. Bruni, P. Lettieri, and F. Maez (2007), Gas retention in fine-grained pyroclastic flow materials at high temperatures, *Bull. Volcanol.*, *69*, 881–901, doi:10.1007/s00445-007-0116-7.

Dufek, J. D., and G. W. Bergantz (2005), Transient two-dimensional dynamics in the upper conduit of a rhyolitic eruption: A comparison of the closure models for the granular stress, *J. Volcanol. Geotherm. Res.*, *143*, 113–132, doi:10.1016/j.jvolgeores.2004.09.013.

Dufek, J., and G. W. Bergantz (2007a), Dynamics and deposits generated by the Kos Plateau Tuff eruption: Controls of basal particle loss on pyroclastic flow transport, *Geochem. Geophys. Geosyst.*, *8*, Q12007, doi:10.1029/2007GC001741.

Dufek, J., and G. W. Bergantz (2007b), The suspended-load and bed-load transport of particle laden gravity currents: Insight from pyroclastic flows that traverse water, *J. Theoret. Comput. Fluid Dyn.*, *21*, 119–145, doi:10.1007/s00162-007-0041-6.

Dufek, J., and M. Manga (2008), The in-situ production of ash in pyroclastic flows, *J. Geophys. Res.*, *113*, B09207, doi:10.1029/2007JB005555.

Dufek, J., M. Manga, and M. Staedter (2007), Littoral blasts: Pumice-water heat transfer and the conditions for steam explosions when pyroclastic flows enter the ocean, *J. Geophys. Res.*, *112*, B11201, doi:10.1029/2006JB004910.

Esposti Ongaro, T. E., A. Neri, G. Menconi, V. de'Michieli, M. P. Marianelli, C. Cavazzoni, G. Erbacci, and P. J. Baxter (2008), Transient 3D numerical simulations of column collapse and pyroclastic density current scenarios at Vesuvius, *J. Volcanol. Geotherm. Res.*, *178*, 378–396, doi:10.1016/j.jvolgeores.2008.06.036.

Fan, J., Y. Ma, X. Zha, and K. Cen (2000), Prediction of dense turbulent particle laden riser flow with a Eulerian and Lagrangian combined model, *Chem. Eng. Commun.*, *179*, 201–218, doi:10.1080/00986440008912196.

Fisher, R. V., G. Orsi, M. Ort, and G. Heiken (1993), Mobility of a large-volume pyroclastic flow-emplacement of the Campanian ignimbrite, Italy, *J. Volcanol. Geotherm. Res.*, *56*, 205–220, doi:10.1016/0377-0273(93)90017-L.

Freundt, A. (2003), Entrance of hot pyroclastic flows into the sea: Experimental observation, *Bull. Volcanol.*, *65*, 144–164.

Gera, D., M. Syamlal, and T. J. O'Brien (2004), Hydrodynamics of particle segregation in fluidized beds, *Int. J. Multiphase Flow*, *30*, 419–428, doi:10.1016/j.ijmultiphaseflow.2004.01.003.

Gidaspow, D. (1994), *Multiphase Flow and Fluidization: Continuum and Kinetic Theory Descriptions*, Academic, Boston, Mass.

Girolami, L., T. H. Druitt, O. Roche, and Z. Khrabrykh (2008), Propagation and hindered settling of laboratory ash flows, *J. Geophys. Res.*, *113*, B02202, doi:10.1029/2007JB005074.

Johnson, W. (1998), The ricochet of spinning and non-spinning spherical projectiles, mainly from water. Part II: An outline of theory and warlike applications, *Int. J. Impact Eng.*, *21*, 25–34, doi:10.1016/S0734-743X(97)00033-X.

Johnson, P. C., and R. Jackson (1987), Frictional-collisional constitutive relations for granular materials, with application to plane shearing, *J. Fluid Mech.*, *176*, 67–93, doi:10.1017/S0022112087000570.

Kneller, B. C., S. J. Bennett, and W. D. McCaffrey (1999), Velocity structure, turbulence and fluid stresses in experimental gravity currents, *J. Geophys. Res.*, *104*, 5381–5391, doi:10.1029/1998JC900077.

Lun, C. K. K., S. B. Savage, D. J. Jeffrey, and N. Chepuniy (1984), Kinetic Theories for granular flow: Inelastic particles in Couette flow and slightly inelastic particles in a general flow field, *J. Fluid Mech.*, *140*, 223–256, doi:10.1017/S0022112084000586.

Mandeville, C. W., S. Carey, and H. Sigurdsson (1996), Sedimentology of the Krakatau 1883 submarine pyroclastic flow, *Bull. Volcanol.*, *57*, 512–529, doi:10.1007/BF00304436.

Miller, T. P., and R. L. Smith (1977), Spectacular mobility of ash flows around Aniakchak and Fisher calderas, Alaska, *Geology*, *5*, 173–176, doi:10.1130/0091-7613(1977)5<173:SMOAFA>2.0.CO;2.

Neri, A., A. Di Muro, and M. Rosi (2002), Mass partition during collapsing and transitional columns by using numerical simulations, *J. Volcanol. Geotherm. Res.*, *115*, 1–18, doi:10.1016/S0377-0273(01)00304-3.

Palladino, D. M., and G. A. Valentine (1995), Coarse-tail vertical and lateral grading in pyroclastic flow deposits of the Latera Volcanic Complex (Vulsini, central Italy): Origin and implications for flow dynamics, *J. Volcanol. Geotherm. Res.*, *69*, 343–364, doi:10.1016/0377-0273(95)00036-4.

Pe-Piper, G., D. J. W. Piper, and C. Perissoratis (2005), Neotectonics and the Kos Plateau Tuff eruption of 161 ka, South Aegean arc, *J. Volcanol. Geotherm. Res.*, *139*, 315–338, doi:10.1016/j.jvolgeores.2004.08.014.

Roche, O., M. A. Gilbertson, J. C. Phillips, and R. S. J. Sparks (2006), The influence of particle size on the flow of initially fluidised powders, *Powder Technol.*, *166*, 167–174, doi:10.1016/j.powtec.2006.05.010.

Rose, W. I., S. Self, P. J. Murrow, C. Bonadonna, A. J. Durant, and G. G. J. Ernst (2008), Nature and significance of small volume fall deposits at composite volcanoes: Insights from the October 14, 1974 Fuego eruption, Guatemala, *Bull. Volcanol.*, *70*, 1043–1067, doi:10.1007/s00445-007-0187-5.

Savage, S. B. (1998), Analyses of slow high-concentration flows of granular materials, *J. Fluid Mech.*, *377*, 1–26, doi:10.1017/S0022112098002936.

Simpson, J. E. (1997), *Gravity Currents in the Environment and the Laboratory*, 2nd ed., 244 pp., Cambridge Univ. Press, Cambridge, U. K.

Sparks, R. S. J., S. N. Carey, and H. Sigurdsson (1991), Sedimentation from gravity currents generated by turbulent plumes, *Sedimentology*, *38*, 839–856, doi:10.1111/j.1365-3091.1991.tb01875.x.

Srivastava, A., and S. Sundaresan (2003), Analysis of a frictional-kinetic model for gas-particle flows, *Powder Technol.*, *129*, 72–85, doi:10.1016/S0032-5910(02)00132-8.

Syamlal, M. (1987), A review of granular stress constitutive relations, *Tech. Rep. DOE/MC/21353-2372*, U.S. Dep. of Energy, Springfield, Va.

Syamlal, M., W. Rogers, and T. J. O'Brien (1993), *MFIX documentation: Theory guide*, 49 pp., U.S. Dep. of Energy, Morgantown, W. Va.

Todesco, M., A. Neri, T. Esposti Ongaro, P. Papale, and M. Rosi (2006), Pyroclastic flow dynamics and hazard in a caldera setting: Application to Phlegrean Fields (Italy), *Geochem. Geophys. Geosyst.*, *7*, Q11003, doi:10.1029/2006GC001314.

Ui, T. (1973), Exceptionally far-reaching, thin pyroclastic flows in southern Kyushu, Japan, *Bull. Volcanol. Soc. Jpn.*, *18*, 153–168.

Valentine, G. A., and K. H. Wohletz (1989), Numerical models of Plinian eruption columns and pyroclastic flows, *J. Geophys. Res.*, *94*, 1867–1887, doi:10.1029/JB094iB02p01867.

Whitham, A. G., and R. S. J. Sparks (1986), Pumice, *Bull. Volcanol.*, *48*, 209–223, doi:10.1007/BF01087675.

J. Dufek, School of Earth and Atmospheric Sciences, Georgia Institute of Technology, 311 Ferst Drive, Atlanta, GA 30332-0340, USA.

M. Manga and J. Wexler, Department of Earth and Planetary Science, University of California, 307 McCone Hall, Berkeley, CA 94720, USA.